

Supporting Information

Pyrido[4,3-*e*][1,2,4]triazolo[4,3-*a*]pyrazines as selective, brain penetrant phosphodiesterase 2 (PDE2) inhibitors

Frederik J. R. Rombouts, Gary Tresadern, Peter Buijnsters, Xavier Langlois, Fulgencio Tovar, Thomas B. Steinbrecher, Greet Vanhoof, Marijke Somers, José-Ignacio Andrés, Andrés A. Trabanco

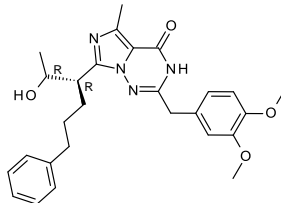
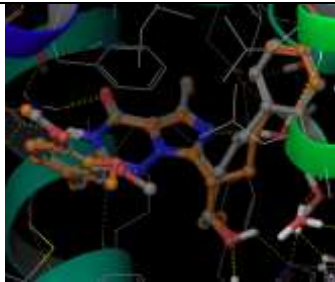
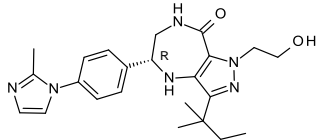
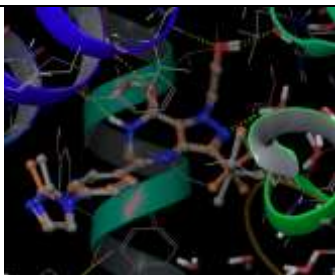
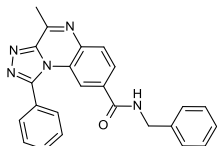
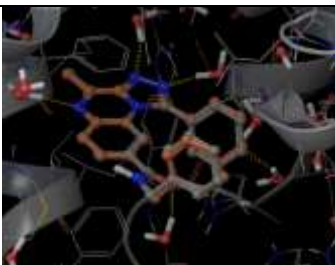
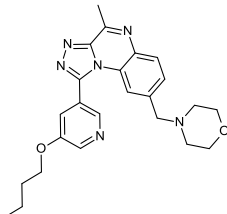
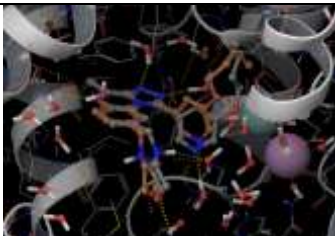
Table of Contents:

1. Computational docking procedure
 2. Free energy perturbation and molecular dynamics calculations
 3. Protocols for measuring inhibition of PDE's in vitro
 4. PDE selectivity profile of **9-15** and **18**
 5. In vivo PDE2 occupancy procedure
 6. Stardrop™ 5 metabolic site predictions for **6**, **9**, **13** and **18**.
 7. Experimental procedures for preparing final compounds **6**, **9-18**
 8. List of abbreviations
 9. References
- 1. Computational Docking Procedure:** Docking was performed using the Glide software (Release 2014-1) from Schrödinger. All protein structures were prepared for docking in the same way, as follows. Firstly, the PDB file was imported into Maestro¹ and structure preparation was performed using the Protein Preparation Wizard² with default settings to fix missing sidechains/atoms, assign protein protonation states with PROPKA, optimize the hydrogen bonding network, assign ligand charges, and relax crystal contacts with a brief minimisation to RMSD 0.5 Å. The ligand was removed and an active site docking grid was calculated using a 30-Å box around Gln859 (alpha carbon). The ligand mid-point box was increased to 20 Å. All active site waters were retained and treated as part of the receptor grid. The active site Gln859 can adopt two rotational conformations, both of which were used for docking with separate receptor grids. No restraints were employed to enforce specific ligand-protein interactions. The Glide SP scoring function was used for docking, but sampling was increased through modifying a number of parameters within Glide: 5000 initial poses, expanded sampling, 1000 best poses retained, and 30 poses per ligand passed to post-docking minimisation. A strain energy correction was applied with the cut-off increased to 6.0 kcal/mol. All other docking parameters were set to the defaults. Molecules were prepared for docking using the LigPrep tool. All default settings were used except ionisation was set at pH 7.4 ± 1.0 to focus the studies on the most energetically favourable states at physiological pH (default is pH 7.0 ± 2.0). Ionisation states of small molecules were also checked by calculating their pK_a at pH 7.4 with the ACD³ software. ConfGen⁴ with fast settings was used to derive multiple 3D conformers for each molecule. All conformers were then passed as input to the Glide SP docking thereby producing multiple docking solutions for each conformer of each molecule. Results were then aggregated at the level of each molecule and the best poses inspected.

The docking protocol was validated by re-docking four different crystallised PDE2 ligand-protein complexes, two from the protein data bank (4HTX⁵ and 4JIB⁶) and two published in our preceding article: 4Do9 (from benzyl ester analogue of **2**) and 4Do8 (from molecule **3**).⁷ The best-ranked docking solutions for each molecule were compared to the experimental structures. The results showed good agreement between docking and X-ray (atom-type colouring atoms). Additional validation (not shown) demonstrated that the docking protocol delivered significant enrichment

to separate known actives from known inactives within a similar MW range. In summary, the docking protocol performed well for predicting the binding mode of ligands from distinct chemical series when docked into the PDE₂ protein structure. For structure based design support and further Free Energy Perturbation calculations, ideas were sketched, minimised and docked into the (3) protein structure (4Do8). This was deemed most suitable as it was solved with a similar ligand from the previous series and had the open lipophilic roof pocket.

Table S1. Validation of the docking protocol by re-docking crystallised ligands into their corresponding protein X-ray structures. The best-docked pose for each molecule is shown in brown/orange colouring and original X-ray coordinates are in atom-type colouring.

pdb	Ligand	Best Docking Solution
4HTX		
4JIB		
4Do9 (Bn amide analogue of 2)		
4Do8 (3)		

2. **Free Energy Perturbation and Molecular Dynamics Calculations:** All calculations were conducted using version 2014-3 of the Schrodinger molecular modeling suite.¹ The FEP+ methodology used here combines an accurate modern force field, OPLS2.1,⁸ the efficient GPU-enabled parallel molecular dynamics engine Desmond version 3.9,⁹ the REST enhanced sampling technique^{10,11} and the cycle-closure correction algorithm¹² to incorporate redundant information into free energy estimates. Calculations were conducted using the FEP mapper technology¹³ to automate setup and analysis. Default computation protocols were used with a 5 ns simulation length for ligands both in complex and in solution, which was extended to 10 ns for the complexes to ensure convergence. For an in-detail description of the free energy calculation protocol employed, consult Ref. 10. As mentioned above, the FEP+ calculations were performed with the molecules bound into the 4Do8 PDE2 crystal structure as starting conformation. In this structure Leu770 adopts an *open* conformation with the α -C β dihedral in the trans-conformation (measured as N-C α -C β -C γ) permitting molecules with larger sidechains to bind. Proteins were prepared as described above for the docking calculations using the Protein Preparation Wizard in Maestro. All resolved crystal water molecules were retained for the free energy simulations. Bound ligand 3D-structures as starting positions for dynamics simulations were placed in their

corresponding receptor binding sites by ligand docking calculations also as described above. Relatively similar ligands for comparison by FEP+ were chosen, since introducing or removing large flexible moieties can result in very slow convergence of the simulations. For instance, compound **14** was initially included in the ligand set, but not analyzed further after the morpholine residue was found to be too large a substituent to include in accurate transformations. Calculations were also performed on molecules **5** and **8** but it is not possible to combine these structural perturbations with those in the meta-position of the phenyl (or pyridyl). The interplay of the latter with the protein conformation (and Leu770 rotation) was our primary interest.

Table S2. Detailed calculation results for FEP+. For each compound, the computed binding free energy ΔG° after 5 ns/lambda of MD simulation time and for 5 ns/lambda of additional sampling are given, to judge simulation convergence. Binding free energies were computed from relative free energy ligand transformation results by adjusting all values by a uniform constant C, to minimize mean unsigned error compared to experiment, since the free energy calculations performed in this work calculate relative binding strengths between similar ligands). Experimental binding free energies were computed approximately from the IC_{50} value, via $\Delta G^\circ = RT \ln(IC_{50})$.

Compound	$\Delta G^\circ_{(exp)}$ [kcal/mol]	$\Delta G^\circ_{(FEP+, 0-5ns)}$ [kcal/mol]	$\Delta G^\circ_{(FEP+, 5-10ns)}$ [kcal/mol]
6	-10.3	-8.1	-8.7
9	-11.2	-11.6	-11.4
10	-9.6	-10.1	-9.9
12	-11.6	-11.7	-11.4
15	-9.3	-9.8	-10.0
16	-7.1	-7.6	-7.5
17	-7.7	-7.8	-8.1

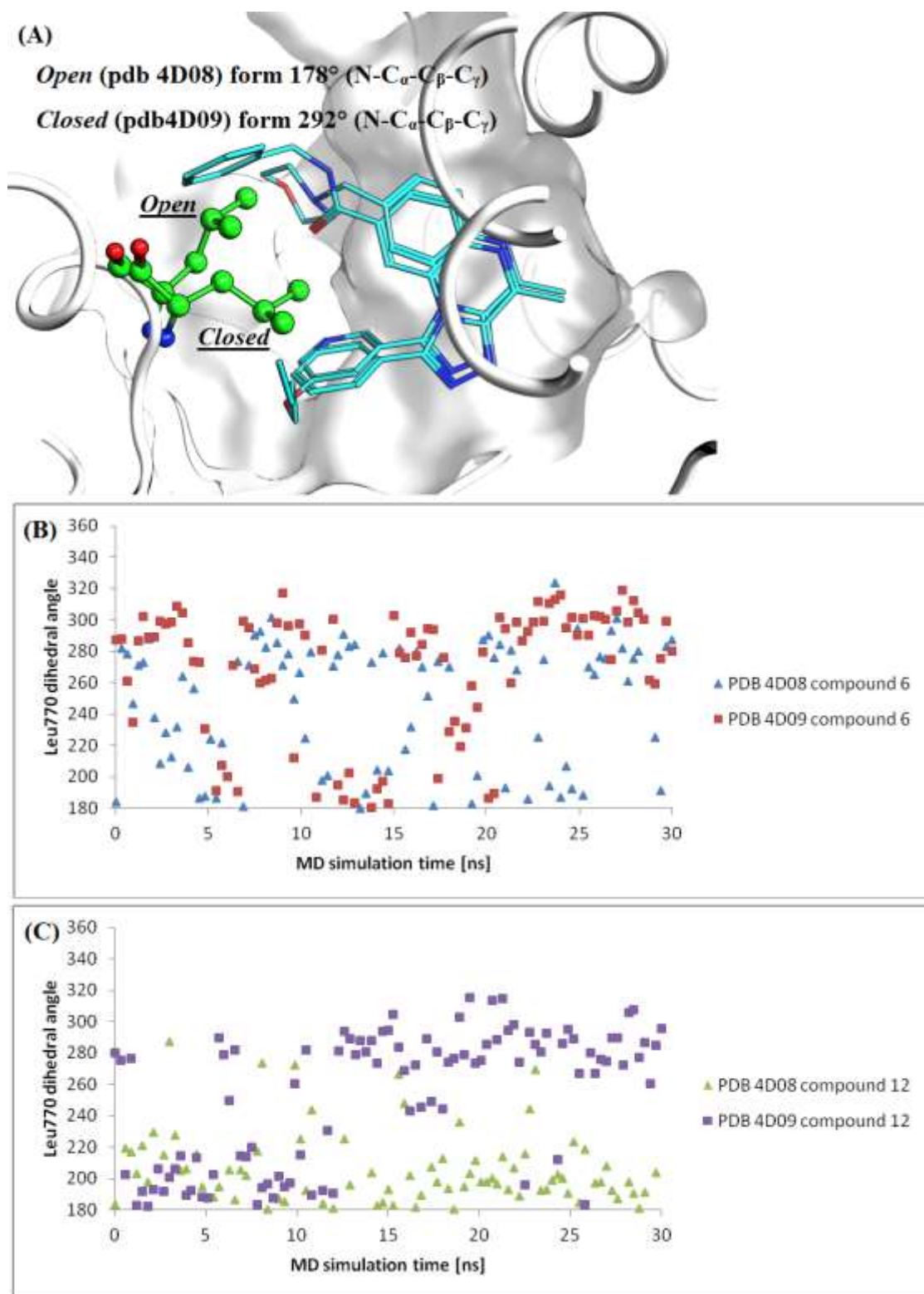
The only large deviation (defined as more than 1 kcal/mol) between experimentally determined and calculated binding affinities occurs for compound **6**, which is found to bind stronger than predicted. Compound **6** is the only one in the ligand set with a phenyl ring without a meta-substituent and in preliminary studies we have observed consistently under-predicted binding affinities for compounds without meta-substituents when comparing to compounds with large substituents (data not shown). The observed deviation is understandable if the protein undergoes a conformational change when binding ligands with differently sized substituents. Such a change has been experimentally observed for the Leu770 binding site residue and has been further explored in MD simulations below.

All atom explicit solvent MD simulations were conducted using the Desmond MD engine, adding a pre-equilibrated box of SPC solvent molecules with a buffer depth of 10 Å for solvation. After an initial standard equilibration protocol, 30 ns of unrestrained MD at 298 K and 1 bar in the NPT ensemble were conducted. Four calculations were performed, simulating two different PDE2 enzyme geometries bound with compounds **6** and **12**. The first is based on PDB 4Do8 in which Leu770 adopts an *open* position with the $C\alpha$ - $C\beta$ dihedral in the trans-conformation (measured as $N-C\alpha-C\beta-C\gamma$). In this conformation the enzyme readily accommodates ligands with a side chain on the phenyl (or pyridyl) ring in the 5-position. For these simulations of PDE2 bound with **12**, Leu770 remained in the *open* conformation over nearly all the duration of the 30 ns simulation (dihedral in trans conformation for 92% of MD simulation snapshots), Figure S1C. However, for ligand **6** which lacks a side chain in the phenyl ring 5-position, Leu770 alternated between the *open* and *closed*

form during the entire simulation (dihedral in *trans* conformation for 47% of MD snapshots), Figure S1B.

The second protein conformation is based on PDB 4D09 and features Leu770 in a gauche *closed* starting conformation. PDE2 was simulated with both **6** and **12** and was observed to alternate between *closed* and *open* form over the simulations. Ligand **12** was found to shift its binding mode to accommodate the slightly smaller binding site pocket it occupies. Although starting from the closed protein conformation Figure S1C shows that during the initial phase of MD simulation Leu770 adopts an open conformation to accommodate the ligand. However, after ~12 ns simulation time ligand **12** moves down in the active site providing sufficient space for Leu770 to revert to a closed conformation. For **6** and **12** respectively, the *closed* forms were observed more frequently, especially for **6** (dihedral in *trans* conformation for 28% of MD snapshots for **6** and 36% for **12**). The results show that the dynamics of Leu770 play a crucial role for the enzyme to accommodate different ligand types and the enzyme exhibits such conformational flexibility on the nanosecond timescale. The results suggest the under-predicted FEP+ binding energy for **6** in the 5-10 ns simulation is due to insufficient sampling to overcome the bias of starting the simulations in the open form of the enzyme.

Figure S1: (A) Alignment of PDE2 structures from 4D08 and 4D09 showing change in Leu770 dihedral conformation. Time series for the C α -C β dihedral angle of Leu770 during 30 ns of unrestrained MD simulations of PDE2 ligand complexes for compound **6** (B) and compound **12** (C). Graphs are labeled with ligand compound and protein pdb starting conformation PDB ID. For compound **6**, both open and closed (*trans* and *gauche*-) positions of the dihedral are observed, while for **12** the open *trans* conformation is seen more frequently.



3. **Protocols for measuring inhibition of PDE's *in vitro*.** Phosphodiesterases 1B1 and 11A4 were expressed in HEK cells from full-length human recombinant clones. Human recombinant phosphodiesterases 2A, 4D3, 5A3, 7A1, 9A1, 10A2, and rat PDE10A2 were expressed in Sf9 cells, using a recombinant baculovirus construct containing the full length sequence containing a 6xHis sequence following the start Met to allow metal affinity purification of the recombinant protein. Cells were harvested and the phosphodiesterase protein was purified by metal chelate chromatography on Ni-sepharose 6FF. PDE6AB, PDE3A and PDE8A were purchased as partially purified Sf9 cell lysates (Scottish Biomedical, UK). All enzymes were diluted in 50 mM Tris pH 7.8, 1.7 mM EGTA, 8.3 mM MgCl₂ except for PDE9A that was diluted in 50 mM Tris pH 7.8, 5 mM MnCl₂ and PDE1B was diluted in 50 mM Tris pH 7.8, 8.3 mM MgCl₂ complemented with 624 U/mL calmodulin and 800 μM CaCl₂. The affinity of the compounds for phosphodiesterases (PDE) was measured by a scintillation proximity assay (SPA). PDE Yttrium Silicate SPA beads allow PDE activity to be measured by direct binding of the primary phosphate groups of non-cyclic AMP or GMP to the beads via a complex iron chelation mechanism. The amount of bound tritiated product (³H]-AMP or [³H]-GMP) was measured by liquid scintillation counting in a TopCount (Packard).

The compounds were dissolved and diluted in 100% DMSO in polystyrene plates to a concentration of 100-fold the final concentration in the assay. Rat PDE10A or human PDE2A enzyme solution (10 μl) was added to 20 μl of incubation buffer (50 mM Tris pH 7.8, 8.3 mM MgCl₂, 1.7 mM EGTA), 10 μl substrate solution consisting of a mixture of non-tritiated and tritiated substrate (to a final concentration of 60 nM cAMP, 0.008 μCi ³H-cAMP for PDE10A, 10 μM cGMP, 0.01 μCi ³H-cGMP for PDE2A), and 0.4 μl compound in 100% DMSO in a 384-well plate, and incubated for 60 or 40 minutes at room temperature for PDE10A and PDE2A respectively. After incubation, the reaction was stopped with 20 μl of stop solution, consisting of PDE SPA beads (17.8 mg beads/mL in 18 mM or 200 mM zinc sulfate for PDE10A or PDE2A respectively). After sedimentation of the beads for 30 minutes, the luminescence was measured in a Perkin Elmer Topcount scintillation counter and results were expressed as counts per minute (cpm). To measure the low control, no enzyme was added to the reaction mixture. The same assay principle was applied for the measurement of the inhibition of other members of the PDE family, with appropriate modifications of enzyme concentration, incubation buffer, substrate solution, incubation time and stop solution. Data were calculated as the percentage of inhibition of total activity measured in the absence of test compound (% control). A best-fit curve was fitted by a minimum sum of squares method to the plot of % control vs compound concentration, from which an IC₅₀ value (inhibitory concentration causing 50 % inhibition of hydrolysis) was obtained.

4. PDE selectivity

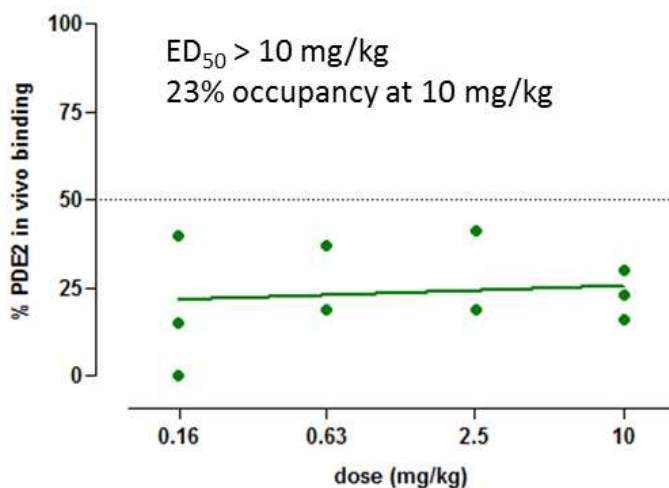
Table S3. PDE2 selectivity profile of profile of compounds 9-15 and 18.^a

Compound	PDE1B IC ₅₀ (nM)	PDE2A IC ₅₀ (nM)	PDE3B IC ₅₀ (nM)	PDE4D IC ₅₀ (nM)	PDE7A IC ₅₀ (nM)	rPDE10A IC ₅₀ (nM)	PDE11 IC ₅₀ (nM)	PDE5A IC ₅₀ (nM)	PDE9A IC ₅₀ (nM)
9	>10000	6	>30200	>10000	>10000	5500	2042	>10000	>10000
10	>10000	95	>10	>10000	>10000	9120	8710	>10000	>10000
11	>30200	21	>30200	n.m.	n.m.	3890	n.m.	n.m.	n.m.
12	n.m.	3	>30200	n.m.	n.m.	2450	n.m.	n.m.	n.m.
13	>10000	10	>30200	>10000	>10000	6030	5370	>10000	>10000
14	n.m.	310	>10000	n.m.	n.m.	>10000	n.m.	n.m.	n.m.
15	n.m.	150	>10000	n.m.	n.m.	8910	n.m.	n.m.	n.m.
18	>10000	54	4467	>10000	>10000	3800	6310	>10000	>10000

^an.m. = not measured

5. **In vivo PDE2 occupancy method.** Male Wistar rats were treated by systemic administration (s.c. or p.o.) of vehicle or different dosages of selective PDE2A inhibitors (n = 3 per dose). After 15 min, every rat received a s.c. injection of the PDE10 inhibitor **MP-10** at the dose of 2.5 mg/kg followed 55 min later by an i.v. injection of the selective PDE2A radioligand [³H]-**3**.^{14,16} Dosing rats with MP-10,^{14,15,16} a potent and selective PDE10 inhibitor, prior to the radioligand injection allowed to increase the signal to noise ratio of [³H]-**3** since its binding is increased when intracellular cGMP concentration raised. Rats were sacrificed 5 min after the tracer injection and their brains dissected and frozen. Then 20 μm thick coronal sections were cut using a cryostat, collected on glass slides and dried. Brain sections were loaded in a β-imager for 12 h. The specific binding was determined as the difference between [³H]-**3** binding quantified in the striatum (a brain area showing a high density of PDE2A) and in the cerebellum (a brain area where PDE2A is virtually absent). Occupancy was calculated as the inhibition of specific [³H]-**3** binding in drug-treated animals relative to vehicle-treated animals. For the determination of the ED₅₀ (dose occupying 50% of PDE2A), the percentage of PDE2A occupancy was plotted against dosage, and the sigmoidal log dose-effect curve of the best fit was calculated by nonlinear regression analysis, using the GraphPad Prism program.

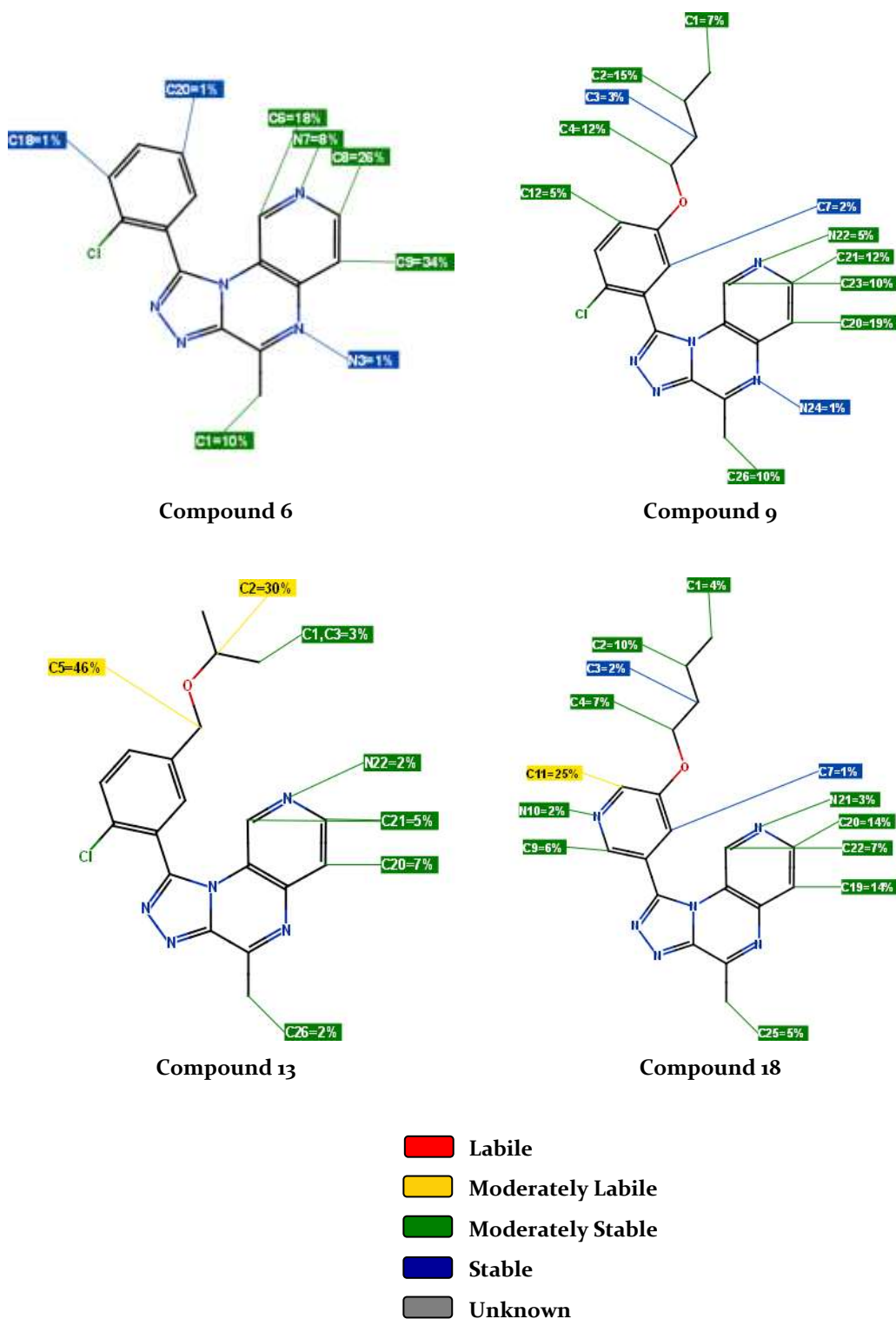
Figure S2. Occupancy data for compound **18** dosed s.c. in rats.



6. Stardrop™ 5 metabolic site predictions

Figure S3 shows the prediction of human CYP_{3A4} metabolism using the StarDrop™ 5 software package for compounds **6**, **9**, **13** and **18**.¹⁹ The side chain pending from the distal phenyl shows moderately labile sites at the adjacent positions to the ether function, whereas for **9** predicted side chain metabolism is lower. The moderate metabolic liability in **18** does not translate into similarly higher metabolism as observed for **13**, which can be explained by the higher intrinsic polarity of **18** (CLogP = 2.8) compared to **13** (CLogP = 4.3).

Figure S3. CYP3A4 metabolism predictions for 6, 9, 13 and 18 using StarDrop™ 5.

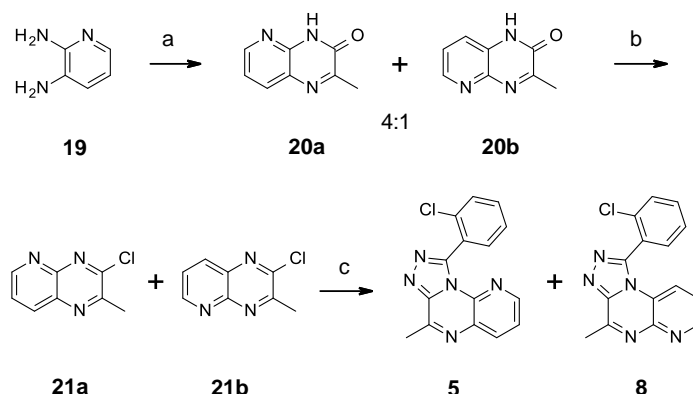


7. Experimental procedures for preparing final compounds 6, 9-18.

Synthetic schemes:

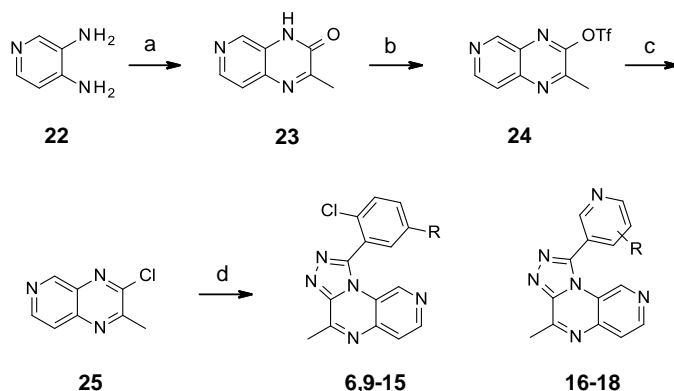
The [1,2,4]triazolo[4,3-*a*]quinoxaline 4 was prepared as described previously.¹⁷ Scheme S1 outlines the synthesis of pyrido[1,2,4]triazolo[4,3-*a*]pyrazines 5 and 8. Reaction of 2,3-diaminopyridine 19 with ethyl pyruvate in MeOH afforded regioisomeric pyrido-pyrazinones 20a and 20b in a 4:1

ratio, as described by Abasolo *et al.*¹⁸ This mixture was treated with POCl₃ to provide the chloro intermediates **21a** and **21b**. The mixture **21a,b** was subsequently treated with 2-chlorobenzohydrazide **26a** yielding the target tricyclic compounds **5** and **8**.



Scheme S1: Reagents and conditions: (a) Ethyl pyruvate, MeOH, rt, 16 h (88%); (b) POCl₃, DIPEA, 1,2-dichloroethane, 80 °C, 1 h (86%); (c) 2-ClC₆H₄CONHNH₂ (**26a**), *n*-BuOH, 160 °C, 35 min (**5**: 10%, **8**: 53%).

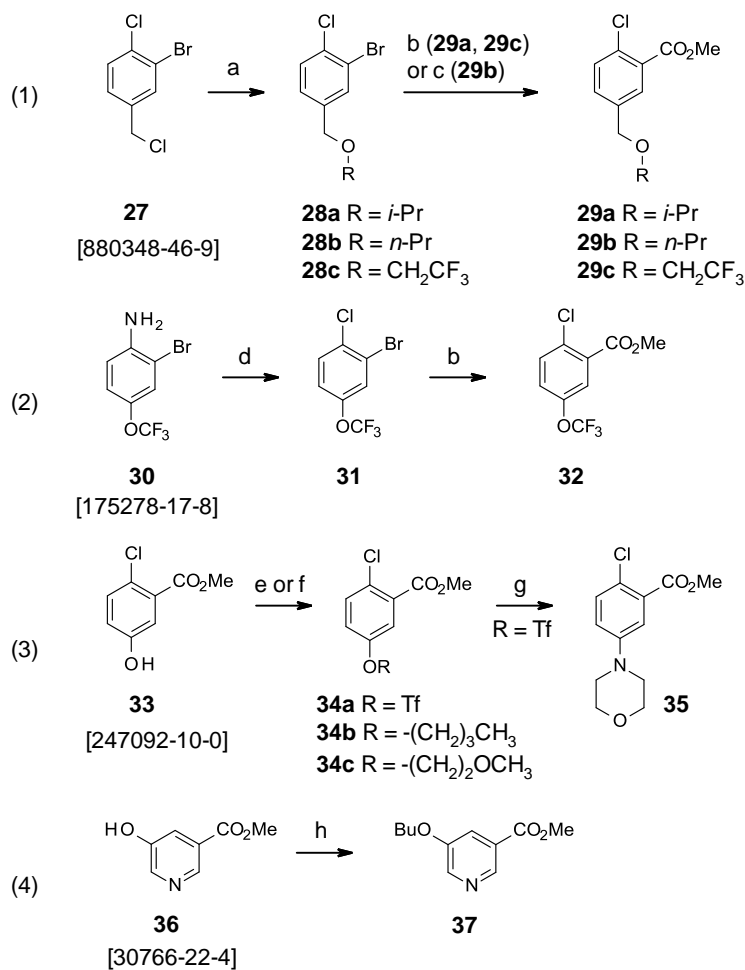
Compounds **6** and **9-18** were obtained similarly starting from 3,4-diaminopyridine **22** (Scheme S2). Again according to observations of Abasolo *et al.*,¹⁸ treating **22** with ethyl pyruvate in CHCl₃ afforded pyrido[3,4-*b*]pyrazin-2-one **23** exclusively. However, attempts to chlorinate **23** with either POCl₃ or SOCl₂ resulted primarily in degradation. Fortunately, reaction of intermediate **23** with triflic anhydride in presence of triethylamine yielded triflate **24**, and subsequent treatment with LiCl in DMSO afforded the key 3-chloropyrido[3,4-*b*]pyrazine **25**. Cyclization with 2-chlorobenzhydrazides **26a-k** finally led to compounds **6** and **9-18**.



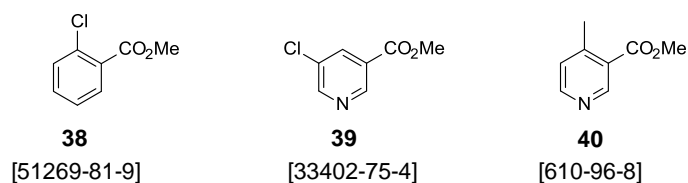
Scheme S2: Reagents and conditions: (a) Ethyl pyruvate, CHCl₃, rt, 16 h (71%); (b) Tf₂O, Et₃N, DMAP, CH₂Cl₂, 5 °C, 2 h (30%); (c) LiCl, DMSO 80 °C, 16 h (37%); (d) (het)ArCONHNH₂ (**26a-k**), *n*-BuOH, 160 °C, 35 min (5-30%).

Benzhydrazides or pyridylhydrazides **26a-k** were synthesized by heating an ethanolic solution of esters **29a-c**, **32**, **34b-c**, **35**, **37-40** with hydrazine hydrate at 85-100 °C overnight (Scheme S4). The esters **29a-c**, **32**, **34b-c**, **35** and **37** were prepared from commercial starting materials as shown in Scheme S3, whereas esters **38-40** were obtained commercially.

Esters synthesized from commercial compounds:

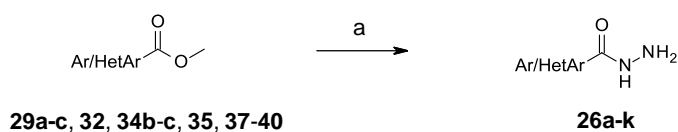


Esters obtained commercially:

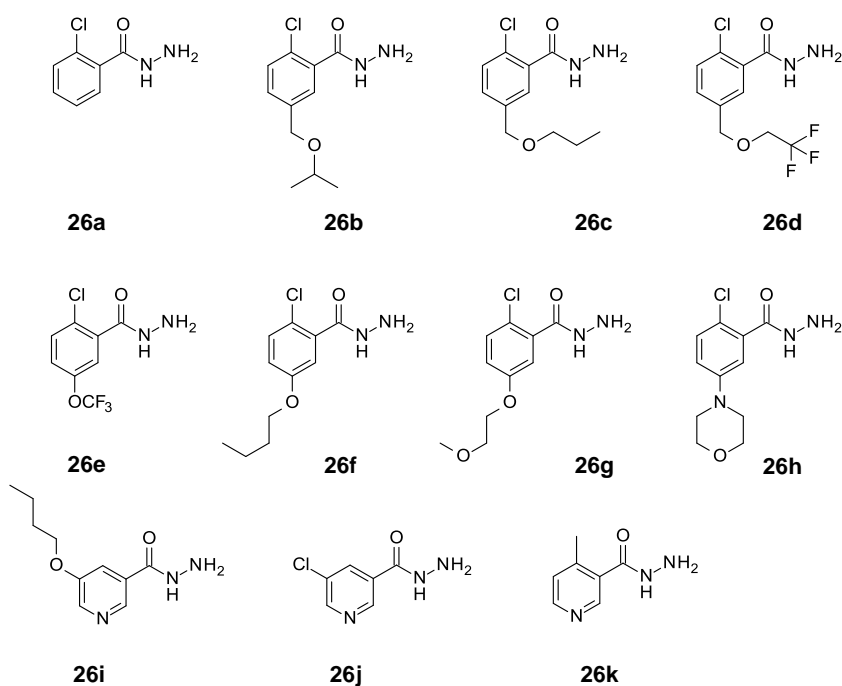


Scheme S3: Reagents and conditions: (a) **28a** and **28c**: ROH, NaH, DMF, 5 °C, 20 min. (**28a**: 73%, **28b**: 83%), or **28b**: *n*-PrOH, K₂CO₃, 120 °C, 12 h (60%); (b) i. *n*-BuLi, CO₂, THF (84%), ii. MeI, K₂CO₃, DMF (40%); (c) CO 6 atm, Pd(OAc)₂, dppf, dioxane-MeOH, 95 °C, 16 h (38-74%); (d) NaNO₂, CuCl, 6 N HCl, 0°C to rt (68%), (e) Tf₂O, Et₃N, DMAP, CH₂Cl₂ (72%); (f) CH₃OCH₂CH₂OH, DIAD, PPh₃, THF, rt (74%); (g) morpholine, Pd₂(dba)₃, Xphos, Cs₂CO₃, PhMe, 100 °C, 2 h (23%); (h) *n*-BuOH, DIAD, PPh₃, THF, rt (65%).

General scheme:



Hydrazides prepared:



Scheme S4: Reagents and conditions: (a) $N_2H_4 \cdot H_2O$, EtOH, 80-100 °C, 12-24 h (75-90%).

Analytical methods:

All final compounds were characterized by 1H NMR and LC/MS. 1H Nuclear Magnetic Resonance spectra were recorded on a Bruker 300 MHz spectrometer, except for **16** and **17**, which were measured on a Bruker 360 MHz spectrometer. For the 1H spectra, all chemical shifts are reported in part per million (δ) units, and are relative to the residual signal at 7.26 and 2.50 ppm for $CDCl_3$ and DMSO, respectively. Compounds **6**, **9**, **12** and **18** were additionally characterized by ^{13}C NMR: **6,9** and **18** on a Bruker 91 MHz spectrometer, and **12** on a Bruker 151 MHz spectrometer.

All the LC/MS analyses were performed using an Agilent G1956A LC/MS quadrupole coupled to an Agilent 1100 series liquid chromatography (LC) system consisting of a binary pump with degasser, autosampler, thermostated column compartment and diode array detector. The mass spectrometer (MS) was operated with an atmospheric pressure electro-spray ionization (API-ES) source in positive ion mode. The capillary voltage was set to 3000 V, the fragmentor voltage to 70 V and the quadrupole temperature was maintained at 100 °C. The drying gas flow and temperature values were 12.0 L/min and 350 °C, respectively. Nitrogen was used as the nebuliser gas, at a pressure of 35 psig. Data acquisition was performed with Agilent Chemstation software.

Analyses were carried out on a YMC pack ODS-AQ C18 column (50 mm long x 4.6 mm I.D.; 3 μ m particle size) at 35 °C, with a flow rate of 2.6 mL/min. A gradient elution was performed from 95% (Water + 0.1% Formic acid)/5% Acetonitrile to 5% (Water + 0.1% Formic acid)/95% Acetonitrile in

4.8 min; the resulting composition was held for 1.0 min; from 5% (Water + 0.1% formic acid)/95% Acetonitrile to 95% (Water + 0.1% formic acid)/5% Acetonitrile in 0.2 min. The standard injection volume was 2 μ L. Acquisition ranges were set to 190-400 nm for the UV-PDA detector and 100-1400 m/z for the MS detector.

Melting points of **6**, **9-15** and **18** were obtained on a Mettler Toledo FP62 capillary melting point apparatus with a gradient 10 $^{\circ}$ C /min and are uncorrected. Melting points of **16** and **17** were measured with differential scanning calorimetry on a Mettler-Toledo-DCS823 apparatus and are uncorrected.

Experimental protocols and analytical data:

*Procedure for the preparation of mixture of isomers 2-methylpyrido[2,3-*b*]pyrazin-3(4*H*)-one **20a** and 3-methylpyrido[2,3-*b*]pyrazin-2(1*H*)-one **20b**:* To a solution of 2,3-diaminopyridine **19** (2 g, 18.32 mmol) in methanol in a round bottom flask (45 mL) was added ethyl pyruvate (2.03 mL, 18.32 mmol). The reaction mixture was stirred at rt overnight. Diisopropyl ether was added and the suspension was stirred at 50 $^{\circ}$ C for 20 min. Then it was allowed to cool to rt and the solid was filtered and dried in an oven at 55 $^{\circ}$ C under vacuum to yield the mixture of isomers **20a** and **20b** (2.1 g, 71%).

*Procedure for the preparation of mixture of isomers 3-chloro-2-methylpyrido[2,3-*b*]pyrazine **21a** and 2-chloro-3-methylpyrido[2,3-*b*]pyrazine **21b**:* To a stirred suspension of isomers **20a** and **20b** (1 g, 6.20 mmol) and diisopropyl ethyl amine (1.05 mL, 6.20 mmol) in DCE (12 mL) in a round bottom flask, POCl₃ (5.78 mL, 6.20 mmol) was added at rt. The reaction mixture was subsequently heated at 90 $^{\circ}$ C for 1 h under nitrogen. The excess of POCl₃ was removed by rotary evaporation and the residue was taken into in DCM and poured into ice-water. Then NH₄OH aq was added until pH = 9, followed by addition of water. The organic layer separated, dried over MgSO₄, filtered and concentrated to dryness. The residue was purified by flash chromatography (20 g silica gel, heptane:EtOAc from 100:0 to 70:30). The product fractions were collected and the solvent evaporated to obtain the mixture of isomers **21a** and **21b** (0.93 g, 86%).

*Procedure for the preparation of mixture of isomers **5** and **8**:* To a suspension of **21a** and **21b** (0.28 g, 1.55 mmol) in *n*-butanol (10 mL) 2-chlorobenzhydrazide (13.36 mmol) was added. The reaction mixture was heated in a closed vessel at 160 $^{\circ}$ C for 35 min. Next, the solvent was evaporated and the residue was taken up in DCM. The organic layer was washed with K₂CO₃ (aq sat.), then dried over MgSO₄ and evaporated to dryness. The crude compound was purified by chromatography (20 g silica gel, DCM:MeOH from 100:0 to 90:10). The fractions containing **5** and **8** were separately collected, concentrated *in vacuo*, and the resulting solids were triturated with diisopropyl ether to give the title compounds as solids.

*9-(2-Chlorophenyl)-6-methylpyrido[3,2-*e*][1,2,4]triazolo[4,3-*a*]pyrazine **5**:* Yield: 10%. LC/MS (*m/z*): 95% pure, R_t = 2.287 min, [M+1]⁺ 296. M.P.: 220.8 $^{\circ}$ C. ¹H NMR (300 MHz, DMSO-*d*₆) δ 8.47 (dd, *J* = 8.1, 1.4 Hz, 1H), 8.44 – 8.38 (m, 1H), 7.75 – 7.63 (m, 4H), 7.61 – 7.51 (m, 1H), 2.96 (s, 3H).

*1-(2-Chlorophenyl)-4-methylpyrido[2,3-*e*][1,2,4]triazolo[4,3-*a*]pyrazine **8**:* Yield: 43%. LC/MS (*m/z*): 97% pure, R_t = 1.906 min, [M+1]⁺ 296. M.P.: 227.3 $^{\circ}$ C. ¹H NMR (300 MHz, DMSO-*d*₆) δ 8.84 (dd, *J* = 4.4, 1.5 Hz, 1H), 7.92 – 7.77 (m, 3H), 7.77 – 7.64 (m, 1H), 7.58 (dd, *J* = 8.4, 4.5 Hz, 1H), 7.49 (dd, *J* = 8.4, 1.6 Hz, 1H), 3.01 (s, 3H).

*2-Methylpyrido[3,4-*b*]pyrazin-3(4*H*)-one **23**:* To a solution of 3,4-diaminopyridine **22** (10 g, 91.63 mmol) in chloroform (100 mL) in a round bottom flask, ethyl pyruvate (51 mL, 458.16 mmol) was added at rt. The reaction mixture was stirred at rt for 16 h. The resulting precipitate was filtered washed with CHCl₃. The resulting solid was suspended in 40 mL diethyl ether and stirred

overnight, after which it was filtered and dried in vacuum to yield **23** as a beige solid (13.00 g, 88%).

2-Methylpyrido[3,4-*b*]pyrazin-3-yltrifluoromethanesulfonate 24: To a suspension of **23** (4.00, 24.82 mmol) in dry DCM were sequentially added triethylamine (6.88 mL, 49.64 mmol) and 4-dimethylaminopyridine (0.152 g, 1.24 mmol). The mixture was cooled to 0 °C and trifluoromethanesulfonic anhydride (6.178 mL, 37.23 mmol) was added portion wise under nitrogen. The mixture was stirred for 2 h at 0 °C and then stirred overnight at rt. Next, the reaction was diluted 50 mL of water and the org layer was separated. The aqueous layer was extracted with 50 mL of DCM. The combined organic layers were washed with brine, dried over MgSO₄ and concentrated in vacuum to give the crude intermediate **24** (2.18 g, 30%).

3-Chloro-2-methylpyrido[3,4-*b*]pyrazine 25: To a solution of **24** (2.18 g, 7.44 mmol) in a mixture of DMSO (100 mL) and THF (70 mL), lithium chloride (1.57 g, 37.22 mmol) was added at rt. The reaction mixture was stirred at 80 °C overnight, after which it was cooled to rt, followed by addition of water and ethyl acetate. The organic phase was separated, dried over MgSO₄ and concentrated *in vacuo*. The crude compound was purified by flash chromatography (30 g silica gel, DCM:EtOAc from 100:0 to 80:20) to give intermediate compound **25** (0.49 g, 37%).

Synthesis of methyl benzoates and methyl nicotines 29a-c, 32, 34b-c, 35, 37-40. The esters **29a-c**, **32**, **34b-c**, **35** and **37** were prepared from commercial starting materials as detailed below and in Scheme S3, whereas esters **38-40** were obtained commercially.

Procedure for the preparation of 3-bromo-4-chlorobenzyl propan-2-yl ether 28a and 3-bromo-4-chlorobenzyl 2,2,2-trifluoroethyl ether 28c: Sodium hydride (60% as a dispersion in mineral oil, 0.8 g, 20.22 mmol) was added portion wise to a solution of 30.33 mmol (3 eq) 2-propanol (for **28a**) or 2,2,2-trifluoroethanol (for **28c**) in dry *N,N*-dimethylformamide (30 mL) at 0 °C. The mixture was stirred at that temperature for 20 min and 2-bromo-1-chloro-4-(chloromethyl)benzene **27** (2.42 g, 10.11 mmol) was added. The mixture was allowed to warm up to room temperature and stirred for 2-6 h. A saturated solution of NH₄Cl (30 mL) and AcOEt (50 mL) were added. The organic phase was washed with brine, dried over MgSO₄ and concentrated *in vacuo*. The crude compound was purified by flash column chromatography (30 g silica gel, heptane:EtOAc from 100:0 to 90:10) to yield intermediate compounds **28a** (83%) or **28c** (73%).

2-Bromo-1-chloro-4-(propoxymethyl)benzene 28b: A mixture of 2-bromo-1-chloro-4-(chloromethyl)benzene (1.14 g, 4.74 mmol) and potassium carbonate (0.65 g, 4.74 mmol) in 1-propanol was heated in a closed vessel at 120 °C overnight. The reaction mixture was cooled, filtered and concentrated *in vacuo*. The crude material was purified by flash column chromatography (30 g silica gel, heptane:EtOAc from 100:0 to 90:10) to give intermediate **28b** (60%).

Procedure for the preparation of methyl 2-chloro-5-[(propan-2-yloxy)methyl]benzoate 29a and methyl 2-chloro-5-[(2,2,2-trifluoroethoxy)methyl]benzoate 29c: A 100-mL, two-necked, bottom flask was equipped with a magnetic stirring was charged with the corresponding aryl bromide (8.58 mmol) and dry THF under nitrogen. The solution was cooled to -78 °C in a dry ice-acetone bath and a solution of *n*-BuLi (2.5 M in hexanes, 3.77 mL, 9.43 mmol) was added via a syringe over 10 min. After the addition was complete, the mixture was stirred for 1 h. The reaction mixture was then poured into solid CO₂ via a cannula under nitrogen atmosphere. The mixture was gradually warmed to room temperature; diluted with water and acidified to pH = 1 with 2 N HCl and finally extracted with AcOEt. The organic phase was separated, dried over MgSO₄ and concentrated *in vacuo* to give the corresponding acid intermediates (7.18 mmol, 84%) as a white solid which was used without further purification.

Methyl iodide (0.47 mL, 7.54 mmol) was added to a stirred suspension of acid intermediate (7.18 mmol) and potassium carbonate (1.48 g, 10.77 mmol) in DMF (21 mL) at room temperature under nitrogen. The mixture was stirred for 2 h at room temperature. Then water (20 mL) and AcOEt (30 mL) were added. The phases were separated and the aq. phase extracted once more. The combined organics were washed with brine, dried over MgSO₄, filtered and evaporated. The crude compound was purified by flash chromatography (30 g silica gel, heptane:EtOAc from 100:0 to 90:10) to give intermediate compounds **29a** (40%) or **29c** (40%).

2-Bromo-1-chloro-4-(trifluoromethoxy)benzene 31: A solution of sodium nitrite (0.81 g, 11.72 mmol) in water (2 mL) was added dropwise to a solution of 2-bromo-4-(trifluoromethoxy)aniline **30** (1.18 mL, 7.81 mmol) in 6 N hydrochloric acid at 5 °C. The mixture reaction was stirred at that temperature for 40 min. Then, a solution of CuCl (1.55 g, 15.62 mmol) in concentrated HCl (3 mL) was added dropwise. The mixture was allowed to warm up to room temperature and stirred for 2-6 h. DCM and water were added and the product was extracted two times. The combined organic layers were dried, filtered and concentrated. The crude compound was purified by flash column chromatography (20 g silica gel, heptane:AcOEt from 100:0 to 85:15) to yield the compound **31** (1.47g, 68%).

Procedure for the preparation of methyl 2-chloro-5-(propoxymethyl)benzoate 29b and methyl 2-chloro-5-(trifluoromethoxy)benzoate 32: A dried steel reaction vessel equipped with a magnetic stirring bar was charged with Pd(OAc)₂ (0.024 g, 0.107 mmol, 2 mol%), dppf (0.11 g, 0.21 mmol, 4 mol%), aryl bromide (5.35 mmol, 1.0 equiv) and triethylamine (2.23 mL, 16.05 mmol, 3.0 equiv), dioxane (20 mL) and methanol (20 mL) and the mixture was charged with nitrogen three times. Then carbon monoxide (excess) was charged (6 atm). The reaction mixture was then stirred at 95 °C overnight. After cooling to room temperature, the reaction mixture was diluted with saturated solution of NaHCO₃ and extracted with ethyl acetate. The organic phase was separated, dried over MgSO₄ and concentrated *in vacuo*. The crude compound was purified by flash chromatography (30 g silica gel, heptane:EtOAc from 100:0 to 90:10) to give intermediate compounds **29b** (38%) and **32** (74%).

Methyl 2-chloro-5-(trifluoromethylsulfonyloxy)benzoate 34a: Triethylamine (6.88 mL, 49.64 mmol) and 4-dimethylaminopyridine (0.152 g, 1.24 mmol) were added to a solution of **33** (0.96 g, 5.14 mmol) in dry DCM under nitrogen. The mixture was cooled to -78 °C and trifluoromethanesulfonic anhydride (1.20 mL, 5.66 mmol) was added portion wise under nitrogen. The mixture was allowed to warm to room temperature for 2 h. The reaction mixture was poured into a saturated solution NH₄Cl (40 mL), the layers were separated. The aqueous layer was extracted twice with dichloromethane. The combined organic fractions were washed with water, dried over MgSO₄ and filtered. The product was purified by a flash column chromatography (20 g silica gel, heptane:AcOEt from 100:0 to 80:20) to afford compound **34a** (1.18 g, 72 %).

Methyl 5-butoxy-2-chlorobenzoate 34b: 1-Bromobutane (1.90 mL, 17.68 mmol) was added to a stirred solution of 2-chloro-5-hydroxybenzoate (3.00 g, 17.08 mmol) and cesium carbonate (5.76 g, 17.68 mmol) in acetonitrile (48 mL). The mixture was subsequently stirred at 55 °C for 4 h, after which water and ethyl acetate were added. The organic phase was separated, dried (MgSO₄), filtered and concentrated to dryness. The residue was purified by flash column chromatography (60 g silica gel, heptane:AcOEt from 100:0 to 96:4). The product fractions were collected and the solvent evaporated to give intermediate **34b** (2.86 g, 73%).

Methyl 2-chloro-5-(2-methoxyethoxy)benzoate 34c: 2-Methoxyethanol (1.50 mL, 19.84 mmol), triphenylphosphine (5.84 g, 22.50 mmol) and DIAD (4.46 mL, 22.50 mmol) were sequentially added to a solution of methyl 2-chloro-5-hydroxybenzoate (3.50 g, 18.75 mmol) in dry THF (100 mL) at 5 °C under nitrogen. The reaction mixture was stirred at room temperature for 2 h. Next,

the reaction mixture was concentrated *in vacuo*. The crude compound was purified by chromatography (60 g silica gel, heptane:AcOEt from 100:0 to 90:10) to give the intermediate **34c** (3.4 g, 74%).

Methyl 2-chloro-5-morpholinobenzoate 35: In a vial equipped with a magnetic stir bar and a screw cap septum was charged **34a** (1.18 g, 4.64 mmol), Pd₂(dba)₃ (0.127 g, 0.14 mmol), Xphos (0.190 g, 0.40 mmol), Cs₂CO₃ (3.02 g, 9.28 mmol) and toluene (20 mL). The mixture was stirred at room temperature while nitrogen was bubbled for 5 min. Then, morpholine (0.49 mL, 5.1 mmol) was added. The reaction was further stirred at 100 °C in a closed vial under nitrogen for 2 h, after which it was cooled to room temperature, and water and AcOEt were added. The organic layer was dried over MgSO₄, filtered and concentrated *in vacuo*. The crude product was purified by flash chromatography (20 g silica, heptane/AcOEt from 100:0 to 80:20). The desired fractions were collected and concentrated *in vacuo* to give compound **35** (0.270 g, 23%).

Methyl 5-butoxynicotinate 37: 1-Butanol (4.30 mL, 47.04 mmol), triphenylphosphine (15.40 g, 58.80 mmol) and DIAD (11.60 mL, 58.80 mmol) were sequentially added to a solution of methyl 5-hydroxynicotinate **36** (6.00g, 39.20 mmol) in dry THF (120 mL) at 5 °C under nitrogen. The reaction mixture was stirred at room temperature for 2 h. The reaction mixture was concentrated *in vacuo*. The crude compound was purified by chromatography (60 g silica gel, heptane: AcOEt from 100:0 to 90:10) to give the intermediate **37** (5.33 g, 65%).

Synthesis of benzhydrazides or pyridylhydrazides 26a-k. Esters **29a-c**, **32**, **34b**, **34c**, **35**, **37-40** (2.90 mmol), hydrazine hydrate (5.80 mmol, 2 eq) and ethanol (5 mL) were mixed in closed vessel under nitrogen atmosphere. The mixture was heated at 85-100 °C overnight. The solvent was evaporated under reduced pressure, and the resulting solid was triturated with heptane, filtered and dried *in vacuo* to give intermediates **26a-k** (75-90% yield, Scheme S4).

General procedure for the preparation of 4-methylpyrido[4,3-*e*][1,2,4]triazolo[4,3-*a*]pyrazines 6, 9-18: To a suspension of **25** (2.40 g, 13.36 mmol) in *n*-butanol (39 mL) the corresponding 2-chloro-4-substituted benzhydrazide or pyridylhydrazide **26a-k** (13.36 mmol) was added. The reaction mixture was heated in a closed vessel at 160 °C for 35 min. Then the solvent was evaporated to dryness and the residue was taken up in DCM. The organic layer was washed with K₂CO₃ (aq sat.), dried over MgSO₄ and evaporated under vacuum. The crude compound was purified by chromatography (20 g silica gel, DCM:MeOH from 100:0 to 90:10). The desired fractions were collected and concentrated *in vacuo*. The resulting solid was triturated with diisopropyl ether or diethyl ether to give the title compound as a solid (5-30%).

1-(2-Chlorophenyl)-4-methylpyrido[4,3-*e*][1,2,4]triazolo[4,3-*a*]pyrazine 6: Yield: 15%. LC/MS (*m/z*): 95% pure, R_t 2.272 min, [M+1]⁺: 296. M.P.: 218.7 °C. ¹H NMR (300 MHz, DMSO-*d*₆) δ 8.75 (d, *J* = 5.3 Hz, 1H), 8.35 (s, 1H), 8.00 (d, *J* = 5.3 Hz, 1H), 7.93 – 7.78 (m, 3H), 7.73 (dd, *J* = 10.4, 3.8 Hz, 1H), 3.00 (s, 3H). ¹³C NMR (91 MHz, DMSO-*d*₆) δ 20.39 (s, 1 C), 121.48 (s, 1 C), 121.64 (s, 1 C), 126.29 (s, 1 C), 127.66 (s, 1 C), 129.37 (s, 1 C), 132.07 (s, 1 C), 132.69 (s, 1 C), 132.84 (s, 1 C), 136.38 (s, 1 C), 139.48 (s, 1 C), 143.79 (s, 1 C), 145.88 (s, 1 C), 147.10 (s, 1 C), 157.45 (s, 1 C).

1-(5-Butoxy-2-chlorophenyl)-4-methylpyrido[4,3-*e*][1,2,4]triazolo[4,3-*a*]pyrazine 9: Yield: 22%. LC/MS (*m/z*): 97% pure, R_t 3.394 min, [M+1]⁺: 368. M.P.: 134.6 °C. ¹H NMR (300 MHz, DMSO-*d*₆) δ 8.76 (d, *J* = 5.4 Hz, 1H), 8.41 (s, 1H), 8.01 (d, *J* = 5.4 Hz, 1H), 7.75 (d, *J* = 8.7 Hz, 1H), 7.45 – 7.32 (m, 2H), 4.13 – 3.97 (m, 2H), 3.00 (s, 3H), 1.81 – 1.61 (m, 2H), 1.53 – 1.34 (m, 2H), 0.92 (t, *J* = 7.4 Hz, 3H). ¹³C NMR (91 MHz, DMSO-*d*₆) δ 12.80 (s, 1 C), 17.78 (s, 1 C), 20.37 (s, 1 C), 29.64 (s, 1 C), 67.26 (s, 1 C), 117.49 (s, 1 C), 118.92 (s, 1 C), 121.59 (s, 1 C), 123.40 (s, 1 C), 126.97 (s, 1 C), 130.29 (s, 1 C), 136.56 (s, 1 C), 139.43 (s, 1 C), 143.65 (s, 1 C), 145.75 (s, 1 C), 147.11 (s, 1 C), 157.22 (s, 1 C), 157.38 (s, 1 C), 165.09 (s, 1 C).

*1-(2-Chloro-5-(2-methoxyethoxy)phenyl)-4-methylpyrido[4,3-*e*][1,2,4]triazolo[4,3-*a*]pyrazine* **10**: Yield: 13%. LC/MS (*m/z*): 96% pure, $R_t = 2.427$ min, $[M+1]^+$: 370. M.P.: 176.2 °C. ¹H NMR (300 MHz, DMSO-*d*₆) δ 8.75 (d, *J* = 5.3 Hz, 1H), 8.45 (s, 1H), 7.98 (d, *J* = 5.3 Hz, 1H), 7.72 (d, *J* = 8.6 Hz, 1H), 7.48 – 7.35 (m, 2H), 4.22 (t, *J* = 4.6 Hz, 2H), 3.69 (t, *J* = 4.6 Hz, 2H), 3.32 (s, 3H), 3.02 (s, 3H).

*1-(2-Chloro-5-(propoxymethyl)phenyl)-4-methylpyrido[4,3-*e*][1,2,4]triazolo[4,3-*a*]pyrazine* **11**: Yield: 16%. LC/MS (*m/z*): 95% pure, $R_t = 3.025$ min, $[M+1]^+$: 368. M.P.: 151.8 °C. ¹H NMR (300 MHz, DMSO-*d*₆) δ 8.75 (d, *J* = 5.3 Hz, 1H), 8.37 (s, 1H), 8.01 (d, *J* = 5.3 Hz, 1H), 7.85 (d, *J* = 8.0 Hz, 1H), 7.82 – 7.72 (m, 2H), 4.61 (s, 2H), 3.45 (t, *J* = 6.5 Hz, 2H), 3.00 (s, 3H), 1.67 – 1.45 (m, 2H), 0.87 (t, *J* = 7.4 Hz, 3H).

*1-(2-Chloro-5-((2,2,2-trifluoroethoxy)methyl)phenyl)-4-methylpyrido[4,3-*e*][1,2,4]triazolo[4,3-*a*]pyrazine* **12**: Yield: 30%. LC/MS (*m/z*): 95% pure, $R_t = 2.941$ min, $[M+1]^+$: 408. M.P.: 184.1 °C. ¹H NMR (300 MHz, DMSO-*d*₆) δ 8.76 (d, *J* = 5.3 Hz, 1H), 8.39 (s, 1H), 8.01 (d, *J* = 5.3 Hz, 1H), 7.89 (d, *J* = 8.0 Hz, 1H), 7.85 – 7.75 (m, 2H), 4.83 (s, 2H), 4.20 (q, *J* = 9.3 Hz, 2H), 3.00 (s, 3H). ¹³C NMR (151 MHz, DMSO-*d*₆) δ 21.18 (s, 1 C), 66.85 (q, *J* = 32.85 Hz, 1 C), 71.76 (s, 1 C), 124.40 (q, *J* = 279.13 Hz, 1 C), 122.27 (s, 1 C), 122.40 (s, 1 C), 127.11 (s, 1 C), 130.20 (s, 1 C), 131.54 (s, 1 C), 132.38 (s, 1 C), 132.73 (s, 1 C), 137.29 (s, 1 C), 137.92 (s, 1 C), 140.27 (s, 1 C), 144.63 (s, 1 C), 146.54 (s, 1 C), 147.90 (s, 1 C), 158.23 (s, 1 C).

*1-(2-Chloro-5-(isopropoxymethyl)phenyl)-4-methylpyrido[4,3-*e*][1,2,4]triazolo[4,3-*a*]pyrazine* **13**: Yield: 12%. LC/MS (*m/z*): 97% pure, $R_t = 2.849$ min, $[M+1]^+$: 368. M.P.: 149.9 °C. ¹H NMR (300 MHz, DMSO-*d*₆) δ 8.75 (d, *J* = 5.3 Hz, 1H), 8.38 (s, 1H), 8.01 (d, *J* = 5.4 Hz, 1H), 7.84 (d, *J* = 8.0 Hz, 1H), 7.80 – 7.72 (m, 2H), 4.61 (s, 2H), 3.80 – 3.62 (m, 1H), 3.00 (s, 3H), 1.17 – 1.13 (m, 6H).

*4-(4-Chloro-3-(4-methylpyrido[4,3-*e*][1,2,4]triazolo[4,3-*a*]pyrazin-1-yl)phenyl)morpholine* **14**: Yield: 5%. LC/MS (*m/z*): 95% pure, $R_t = 2.469$ min, $[M+1]^+$: 381. ¹H NMR (300 MHz, DMSO-*d*₆) δ 8.76 (d, *J* = 5.4 Hz, 1H), 8.44 (s, 1H), 8.01 (d, *J* = 5.4 Hz, 1H), 7.66 (d, *J* = 8.7 Hz, 1H), 7.43 – 7.31 (m, 2H), 3.79 – 3.68 (m, 4H), 3.26 – 3.16 (m, 4H), 3.00 (s, 3H).

*1-(2-Chloro-5-(trifluoromethoxy)phenyl)-4-methylpyrido[4,3-*e*][1,2,4]triazolo[4,3-*a*]pyrazine* **15**: Yield: 9%. LC/MS (*m/z*): 96% pure, $R_t = 2.998$ min, $[M+1]^+$: 380. M.P.: 135.1 °C. ¹H NMR (300 MHz, CDCl₃-*d*₃) δ 8.79 (d, *J* = 5.4 Hz, 1H), 8.69 (s, 1H), 7.94 (d, *J* = 5.3 Hz, 1H), 7.71 (d, *J* = 8.8 Hz, 1H), 7.61 (d, *J* = 2.7 Hz, 1H), 7.55 (dd, *J* = 8.8, 2.1 Hz, 1H), 7.26 (s, 3H), 3.15 (s, 3H).

*1-(5-Chloropyridin-3-yl)-4-methylpyrido[4,3-*e*][1,2,4]triazolo[4,3-*a*]pyrazine* **16**: Yield: 8%. LC/MS (*m/z*): 99% pure, $R_t = 1.648$ min, $[M+1]^+$: 297. M.P.: 225.29 °C. ¹H NMR (360 MHz, DMSO-*d*₆) δ 3.00 (s, 3 H), 8.02 (d, *J* = 5.5 Hz, 1 H), 8.52 – 8.55 (m, 1 H), 8.72 (s, 1 H), 8.77 (d, *J* = 5.49 Hz, 1 H), 9.01 (d, *J* = 1.83 Hz, 1 H) 9.03 (d, *J* = 2.6 Hz, 1 H).

*4-Methyl-1-(4-methylpyridin-3-yl)pyrido[4,3-*e*][1,2,4]triazolo[4,3-*a*]pyrazine* **17**: Yield: 11%. LC/MS (*m/z*): 99% pure, $R_t = 1.337$ min, $[M+1]^+$: 277. M.P.: 252.90 °C. ¹H NMR (360 MHz, DMSO-*d*₆) δ 2.19 (s, 3 H), 3.00 (s, 3 H), 7.66 (d, *J* = 5.1 Hz, 1 H), 8.00 (d, *J* = 5.1 Hz, 1 H), 8.33 (s, 1 H), 8.74 (d, *J* = 5.1 Hz, 1 H), 8.78 (s, 1 H), 8.82 (d (br), *J* = 4.4 Hz, 1 H).

*1-(5-Butoxypyridin-3-yl)-4-methylpyrido[4,3-*e*][1,2,4]triazolo[4,3-*a*]pyrazine* **18**: Yield: 10%. LC/MS (*m/z*): 95% pure, $R_t = 2.584$ min, $[M+1]^+$: 334. M.P.: 161.3 °C. ¹H NMR (300 MHz, CDCl₃-*d*₃) δ 8.98 (s, 1H), 8.78 (d, *J* = 5.3 Hz, 1H), 8.62 (d, *J* = 2.8 Hz, 1H), 8.57 (d, *J* = 1.7 Hz, 1H), 7.93 (d, *J* = 5.3 Hz, 1H), 7.56 – 7.47 (m, 1H), 4.09 (t, *J* = 6.4 Hz, 2H), 3.13 (s, 3H), 1.92 – 1.76 (m, 2H), 1.54 – 1.43 (m, 2H), 0.99 (t, *J* = 7.4 Hz, 3H). ¹³C NMR (91 MHz, DMSO-*d*₆) δ 12.78 (s, 1 C), 17.74 (s, 1 C), 20.31 (s, 1 C), 29.58 (s, 1 C), 67.31 (s, 1 C), 120.08 (s, 1 C), 120.96 (s, 1 C), 121.54 (s, 1 C), 121.80 (s, 1 C), 123.99 (s, 1 C), 137.19 (s, 1 C), 139.62 (s, 1 C), 139.96 (s, 1 C), 140.73 (s, 1 C), 144.03 (s, 1 C), 146.20 (s, 1 C), 146.78 (s, 1 C), 153.89 (s, 1 C), 157.09 (s, 1 C).

8. List of abbreviations:

pdb, protein data bank (<http://www.rcsb.org/pdb/home/home.do>); EGTA, ethylene glycol tetraacetic acid; cAMP, cyclic adenosine monophosphate; cGMP, cyclic guanosine monophosphate; IC₅₀, concentration giving 50% inhibition; ED₅₀, dose giving 50% effect; DCE, 1,2-dichloroethane; dppf, 1,1'-Bis(diphenylphosphino)ferrocene; DIAD, Diisopropyl azodicarboxylate; DMAP, 4-Dimethylaminopyridine; Xphos, 2-Dicyclohexylphosphino-2',4',6'-triisopropylbiphenyl;

9. References:

1. Schrodinger LLC, 120 West 45th Street 17th Floor, Tower 45 New York, NY 10036-4041, USA at <http://www.schrodinger.com/Maestro/2014> (accessed Dec 19, 2014).
2. Sastry, G. M.; Adzhigirey, M.; Day, T.; Annabhimoju, R.; Sherman, W. Protein and ligand preparation: parameters, protocols, and influence on virtual screening enrichments. *J. Comp. Aided Mol. Des.* **2013**, *27*, 221-234.
3. ACD Labs software. pKa v12.0. Advanced chemistry development Inc. 110 Yonge Street, 14th Floor, Toronto, Ontario, Canada, M5C 1T4. <http://www.acdlabs.com/home> (accessed Dec 19, 2014).
4. Watts, K. S.; Dalal, P.; Murphy, R. B.; Sherman, W.; Friesner, R. A.; Shelley, J. C. ConfGen: A Conformational Search Method for Efficient Generation of Bioactive Conformers. *J. Chem. Inf. Model.* **2010**, *50*, 534-546.
5. Zhu, J.; Yang, Q.; Dai, D.; Huang, Q. X-ray crystal structure of phosphodiesterase 2 in complex with a highly selective, nanomolar inhibitor reveals a binding-induced pocket important for selectivity. *J. Am. Chem. Soc.* **2013**, *135*, 11708-11.
6. Plummer, M. S.; Cornicelli, J.; Roark, H.; Skalitzky, D. J.; Stankovic, C. J.; Bove, S.; Pandit, J.; Goodman, A.; Hicks, J.; Shahripour, A.; Beidler, D.; Lu, X. K.; Sanchez, B.; Whitehead, C.; Sarver, R.; Braden, T.; Gowan, R.; Shen, X. Q.; Welch, K.; Ogden, A.; Sadagopan, N.; Baum, H.; Miller, H.; Banotai, C.; Spessard, C.; Lightle, S. Discovery of potent, selective, bioavailable phosphodiesterase 2 (PDE2) inhibitors active in an osteoarthritis pain model, part I: transformation of selective pyrazolodiazepinone phosphodiesterase 4 (PDE4) inhibitors into selective PDE2 inhibitors. *Bioorg. Med. Chem. Lett.* **2013**, *23*, 3438-42.
7. Buijnsters, P.; Andrés, J.-I.; De Angelis, M.; Langlois, X.; Rombouts, F.; Sanderson, W.; Tresadern, G.; Ritchie, A.; Trabanco, A.; Vanhoof, G.; Van Roosbroeck, Y. Structure-Based Design of a Potent, Selective, and Brain Penetrating PDE2 Inhibitor with Demonstrated Target Engagement. *ACS Med. Chem. Lett.* **2014**, *5*, 1049-1053.
8. Shivakumar, D.; Harder, E.; Damm, W.; Friesner, R. A.; Sherman, W. Improving the Prediction of Absolute Solvation Free Energies Using the Next Generation OPLS Force Field. *J. Chem. Theory Comput.* **2012**, *8*, 2553-2558.
9. Bowers, K. J.; Chow, E.; Xu, H.; Dror, R. O.; Eastwood, M. P.; Gregersen, B. A.; Klepeis, J. L.; Kolossvary, I.; Moraes, M. A.; Sacerdoti, F. D.; Salmon, J. K.; Shan, Y.; Shaw, D. E. Scalable Algorithms for Molecular Dynamics Simulations on Commodity Clusters. *Proceedings of the 2006 ACM/IEEE conference on Supercomputing; ACM: Tampa, Florida*, **2006**, 84.
10. Liu, P.; Kim, B.; Friesner, R. A.; Berne, B. J. Replica exchange with solute tempering: a method for sampling biological systems in explicit water. *Proc. Nat. Acad. Sci. USA* **2005**, *102*, 13749-13754.
11. Wang, L.; Friesner, R. A.; Berne, B. J. Replica exchange with solute scaling: a more efficient version of replica exchange with solute tempering (REST2). *J. Phys. Chem. B* **2011**, *115*, 9431-9438.
12. Wang, L.; Deng, Y.; Knight, J. L.; Wu, Y.; Kim, B.; Sherman, W.; Shelley, J. C.; Lin, T.; Abel, R. Modeling local structural rearrangements using FEP/REST: Application to relative binding affinity predictions of CDK2 inhibitors. *J. Chem. Theory Comput.* **2013**, *9*, 1282-1293.

13. Liu, S.; Wu, Y.; Lin, T.; Abel, R.; Redmann, J.; Summa, C.; Jaber, V.; Lim, N.; Mobley, D. Lead optimization mapper: automating free energy calculations for lead optimization. *J. Comput.-Aided Mol. Des.* **2013**, *27*, 755-770.
14. Verhoest, P. R.; Chapin, D. S.; Corman, M.; Fonseca, K.; Harms, J. F.; Hou, X.; Marr, E. S.; Menniti, F. S.; Nelson, F.; O'Connor, R.; Pandit, J.; Proulx-Lafrance, C.; Schmidt, A. W.; Schmidt, C. J.; Suiciak, J. A.; Liras, S. Discovery of a novel class of phosphodiesterase 10A inhibitors and identification of clinical candidate 2-[4-(1-methyl-4-pyridin-4-yl-1*H*-pyrazol-3-yl)-phenoxy-methyl]-quinoline (PF-2545920) for the treatment of schizophrenia. *J. Med. Chem.* **2009**, *52*, 5188-96.
15. Andrés, J.-I.; Buijnsters, P.; De Angelis, M.; Langlois, X.; Rombouts, F.; Trabanco, A. A.; Vanhoof, G. Discovery of a new series of [1,2,4]triazolo[4,3-*a*]quinoxalines as dual phosphodiesterase 2/phosphodiesterase 10 (PDE2/PDE10) inhibitors. *Bioorg. Med. Chem. Lett.* **2013**, *23*, 785-790.
16. Walker, M. A. Discovery of PDE10A inhibitor, PF-2545920. *Drug Discov. Today* **2010**, *15*, 79.
17. Andrés-Gil, J. I.; Rombouts, F.; Trabanco-Suárez, A.; Vanhoof, G.; De Angelis, M.; Buijnsters, P.; Guillemont, J.; Bormans, G.; Celen, S.; Vliegen, M. Preparation of (un)labeled 1-aryl-4-methyl-[1,2,4]triazolo[4,3-*a*]quinoxaline derivatives as PDE2 and PDE10 inhibitors for therapy and imaging, PCT Int. Appl. (2013), WO 2013000924 A1.
18. Abasolo, M. I., Bianchi, D., Atlasovich, F., Gaozza, C. and Fernández, B. M. (1990), Kinetic study on the anelation of heterocycles. 2. pyrido[2,3-*b*]pyrazine and pyrido[3,4-*b*]pyrazine derivatives synthesized by the Hinsberg reaction. *J. Heterocyclic Chem.* **1990**, *27*, 157-162.
19. StarDrop™ is a trademark of Optibrium, Ltd., 7221 Cambridge Research Park, Beach Drive, Cambridge, CB25 9TL, UK. <http://www.optibrium.com> (accessed Dec 19, 2014).